Periodical oscillation of particle-laden laminar flow within a tubular photocatalytic hydrogen production reactor predicted by DEM simulation

JiafengGeng[1], Junwang Tang[2], Wenfang Cai[3,4], Yechun Wang[1], Dengwei Jing[1,*],Liejin Guo[1]

1. State Key Laboratory of Multiphase Flow in Power Engineering & International Research Center for Renewable Energy, Xi'an Jiaotong University Xi'an 710049, China
2. Department of Chemical Engineering, University College London, WC1E 7JE, UK
3. School of Chemical Engineering and Technology, Xi'an Jiaotong University, Xi'an, Shaanxi 710049, China
4. Department of Environmental Science and Technology, Xi'an Jiaotong University, Xi'an, Shaanxi 710049, China

* Corresponding author: Tel.:+86-29-82668769; Email: dwjing@mail.xjtu.edu.cn

Abstract

Besides their wide existence in various industrial processes, nanoscale particle suspensions are also the important media for some emerging technologies such as photocatalytic hydrogen production. The circulating flow properties of the nanoparticles in the fluid are of great concern for their practical use. In our study, a modified experimental system was set up based on Malvern laser particle analyzer that can estimate the nanoparticle concentration and size distribution in a laminar nanoparticle circulating flow. We found that the particle concentration and size distribution were periodical oscillation with time in such flow. Understanding the oscillation mechanism is capable of promote the energy efficiency of photocatalytic hydrogen production. A simulation based on Discrete Element Method (DEM) was conducted to understand this particular oscillation mechanism by counting the single particle movement and trajectory properties in the solid-liquid suspension. The simulation results agree well with the tendency obtained by the experimental results and capable of better understanding the oscillation characteristics. The simulation results reveal that the nanoparticles tend to gather in the middle region (the higher velocity region) of the tube after several cycles. Moreover the gravity is of great significance in the circulating flow of solid-liquid suspension because the particle swarms tend to distribute a little below the axial center line of the straight tube. These obtained results are credible for understanding the nanoscale particle transport phenomenon in many natural or industrial processes. In particular, our results are helpful for the understanding and effective control of the movement

and distribution of photocatalyst particles in the tubular photocatalytic reactor, which is believed to significantly affect the incident radiation distribution and finally the energy conversion efficiency of the photocatalytic process.

Key Words: particle-laden flow, DEM simulation, periodical oscillation, particles trajectory

1. Introduction

The suspensions of micro- or nanoscale particles in liquid exist widely in various fields, e.g. advanced material processing, electronic technology, chemical engineering, petroleum, food processing, waste treatment etc. It is also the important media for some emerging technologies such as the enhancement of heat transfer, photocatalytic energy conversion and environmental remediation [1-4]. In all of these processes, the particle transportation and deposition have significant impact on the properties application promotion of such kind of suspension. For example, in photocatalytic process, sedimentation of the photocatalyst which leading to ineffective light absorption must be avoided [5]. For another example, in nanofluids heat transfer enhancement, the deposition of nanoparticles will change the wettability of the heater surface, thus affecting the overall heat transfer performance [6].

Photocatalytic hydrogen production from water splitting using solar energy is one of the ultimate reactions to solve energy and environmental issues [7].In order to realize the industrial application of photocatalytic hydrogen production technology, a large number of studies have been carried out in the past twenty years. And there are two main research fields, one is the exploration for efficient visible light driven photocatalyst [5,8-12], the other one is the development of high efficiency photocatalytic reactors [13-17]. As the photocatalyst has been studied for many years, and the quantum efficiency of the photocatalyst has reached 93% with noble metal loading [18] and reached 62% without noble metal loading[19], whereas the energy conversion efficiency is still not able to exceed 5% in present [20,21]. It is believed that the great difference between the above two efficiencies is due to the inefficient utilization of the light in the photocatalytic reactor. And the suspension state and transport phenomenon of photocatalytic particles in the reactor has significant impact on the absorption of light; as a result, determine the overall energy conversion efficiency of the photocatalytic reaction.

For the clearer understanding of the transportation phenomenon in nanoparticle flow, many studies have been conducted by means of experimental and/or numerical method. In experimental study, one mainly concerns about the concentration distribution, velocity distribution and particle size distribution, and the experimental methods mainly include intrusive and non-intrusive method. Sampling method[22] and probe method[23-25] are two most frequently-used methods in the intrusive method. Although this kind of method is easy to use and intuitive, it inevitably disturbs the flow field due to the existence of sampling equipment and probe. To overcome this defect, some non-intrusive methods have been developed, such as the light technique [26], radiation technique[27], ultrasonic attenuation techniques [28], tomographic technique[29] etc. Among these techniques, light technique is the most widely used technique, for it is convenient, safe, and responsive and has simple structure. Laser diffraction (LD) technique is a kind of light technique based on the light diffraction by particles, which has become a popular method to measure the particle size and concentration distribution [30,31], due to its high speed, good reliability and high reproducibility [32].

Although many experimental methods have been developed, they still have some limitations, such as low accuracy, high cost, disturbance to the flow field etc. Also, Numerical methods have been employed as a very important supplementary method to give insight into the particle distribution and flow characteristics in the particle suspensions. In general, simulation of the solid-liquid suspension can be conducted by either continuum or discrete methods, depending on the time and length scales employed for solid phase. The former is often based on the two-fluid model (TFM), whereas the latter is usually based on the discrete element method (DEM). Very often, the discrete phase method (DPM) coupled with computational fluid dynamics (CFD) have been used, which gives the DPM-CFD or combined continuum and discrete model (CCDM). TFM is available to study the fluid mixture movement as a whole and the phase distribution. Hu et al. [33] investigated the effects of the slurry flow and catalyst distributions in the reactor on photocatalysis for hydrogen production with an algebraic slip mixture model (ASM). Hatami et al. [34] studied steady and unsteady magneto-hydrodynamic (MHD) Couette flows between two parallel infinite plates with a two-fluid model through numerical Differential Quadrature Method (DQM) and analytical Differential Transformation Method (DTM), respectively. The forced convection of laminar TiO_2–water nanofluid flow in a parallel plate microchannel has been studied by a modified homogeneous flow model and the dispersion model [35]. Although the TFM model is used widely and suitable to most two-phase flow problems, some detailed particle-scale information might be missed, such as the trajectories and forces acting on individual particles, which are very significant to explain the mechanisms governing the complicated flow behavior. CCDM has thus been increasingly used for studying various solid-liquid flow phenomena [36]. Morris and Brady [37] studied the pressure-driven flow of a non-neutrally buoyant suspension by the suspension-balance model of NB considering the particles migration which is a DEM model. Peng et al. [38] investigated the influence of primary particle size distribution (PPSD) on aggregation behavior and the resulting effect on yield stress of a concentrated colloidal suspension with DEM model. Chaumeil and Crapper [39] investigated the agglomeration and deposition on a constricted tube collector of colloidal size particles immersed in a liquid.

The literature review above indicate that most of the studies by DEM modeling are conducted in a one-way channel, which means the particle suspension will pass the channel for only one time in simulation. Whereas in many photocatalytic reactors, nanoparticle suspensions are in fact circulated in a loop, considering that such flowing reactor is cost-effective, easy for scale-up and for nanoparticles recycling [40-44].

In particular, sequencing batch reactor (SBR) is commonly used in photocatalytic technology to decrease the consumption of pump power [16,45]. And particles need to be resuspension after a period of time when the SBR photocatalytic reactor is in operation, so it is very important to know the real process of particles spreading with the suspension flow. Thus, a initial condition that particles added at the beginning was select to simulate the process. And in the circulating flow, the gravity cannot be neglected considering that the particles in solid-liquid suspension will keep moving in the reactor under the action of gravity [46]. And the equilibrium position of the particles after enough times of circulating flow should be of great interest in photocatalytic application, for it is extremely important to know the location and of particles in the photocatalytic reactor which has great impact on the light absorption. Therefore, the equilibrium position of these particles is also discussed in this study. In our previous study, an experimental research is conducted to investigate the changes of particles concentration and size distribution with time during the circulating flow. In this study, a DEM two-way coupling model was employed to obtain the details of particles migration and also the key macroscopic parameters for comparison with experimental results. This model focused on understanding the periodical oscillation of particle concentration and size distribution with time in such circulating flow. The particle volume fraction, the flow field of the particle-laden flow in the circulating flow system, the particle trajectory and the particle size spatial distribution were discussed by this model. This model provides an intuitive and credible insight on the periodical oscillation mechanism of photocatalyst particles tubular photocatalytic reactor, and eventually explains incident radiation distribution and the energy conversion efficiency of the photocatalytic process.

2. Experimental set-sup and materials

In our previous work, we had established an experimental set-up as has been shown in **Fig 1** [47]. It has six parts: main flow channel, centrifugal pump, wet sample injector, laser particle analyzer and connecting tube. The main flow channel working as test section in this study is made from acrylic glass and has an inner diameter of 30 mm and a total length of 0.5 m which is transparent. Connecting tube is the silicone hose which the inner diameter is 10mm, and the total length of it is 1.7 m. The centrifugal pump is used to provide driving power of the circulating flow. A Malvern Spraytec laser particles analyzer was used to monitor particle concentration and particles size distribution simultaneously. Degussa P25 titanium dioxide was employed as model particles and main parameters for this widely used photocatalyst, and the specifications of P25 TiO2 powder can be found in Ref. [48]. Again, it is worth mentioning that photocatalytic energy conversion is a very attractive technology for which one of the key issues is the well-suspension of the particles in the reactor [3,49,50]. A very low flow velocity may result in the sedimentation of particles while a too high flow velocity could lead to a significantly reduced exposure time of the photocatalyst to solar light. One must guarantee that all the useful incoming photons are used and do not escape without having intercepted a particle in the reactor [3,51]. In our design, the average volume fraction of nanoparticles is $\varphi=1\times10^{-4}$ in the tube. It can thus be considered as a dilute flow and the possible interactions between particles can be safely ignored during theoretical analysis.

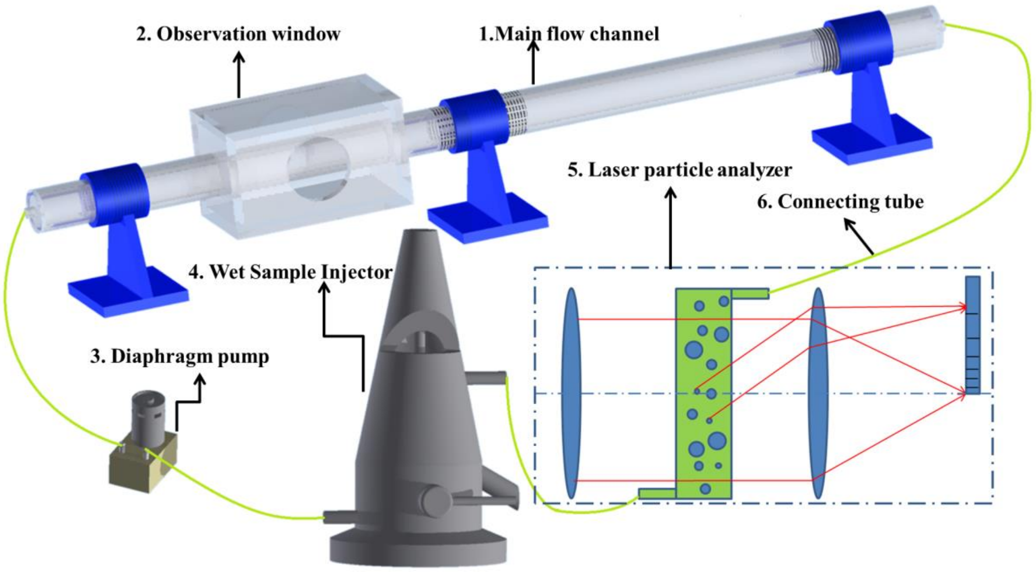

Fig.1. Schematic of experiment set-up[47]

Firstly, the system was filled with deionized water and circulated by pump with the flowrates adjusted to 15 L/h. And the P25 particles are dispersed in deionized water in previous, which the particle size distribution is showed in **Fig. 2a**. And it can be seen that the range of the particle diameter is 0.50-36.87μm. Then the prepared P25-TiO_2 suspension was introduced into the wet sample injector and the laser diffraction equipment starts to record the particles volume fraction and size distribution simultaneously. **Fig.2b** shows the mean particle size and concentration versus time in the repeatedly circulating flow. Here, the upper two curves corresponds to the variations of two kinds of mean particle sizes, D_{32} and D_{43}, respectively and the bottom curve corresponds to the variation of particles volume fraction against time. Here, D_{32} is the mean particle size taking into account both volume and surface area of the particles [52], while the D_{43} is the average particle size based on the volume moment [53]. The corresponding expression for the two average particle sizes can be derived respectively by:

$$\boldsymbol{D_{32}} = \frac{\sum V_i D_i^3}{\sum V_i D_i^2} \tag{1}$$

$$\boldsymbol{D_{43}} = \frac{\sum V_i D_i^4}{\sum V_i D_i^3} \tag{2}$$

Obvious periodic oscillation of both mean particle sizes and particles volume fraction with time can be noted in **Fig.2b**. And we can define the distance between two adjacent peaks as the period of the oscillation curve. It can be found that the period of the three curves in the **Fig. 2b** is nearly the same. The oscillation of the particle volume fraction curve with time is particularly significant in the initial 600 seconds, and after that the particle volume fraction of the particles in suspension tends to be a constant value, which we define this state as quasi-steady state. According to the definition of mean particle size and D_{43}, D_{43} is more sensitive to the large particles, while smaller particles contribute more to the D_{32}. It is also noted in the **Fig. 2b** that the D_{32} and D_{43} curves are also oscillation curves, but the tendency of them are some different comparing to the particle volume fraction curve. It can be observed that the particle volume fraction curve fluctuates around an average value, while the D_{43} and D_{32} curves fluctuate with an obviously downward trend.

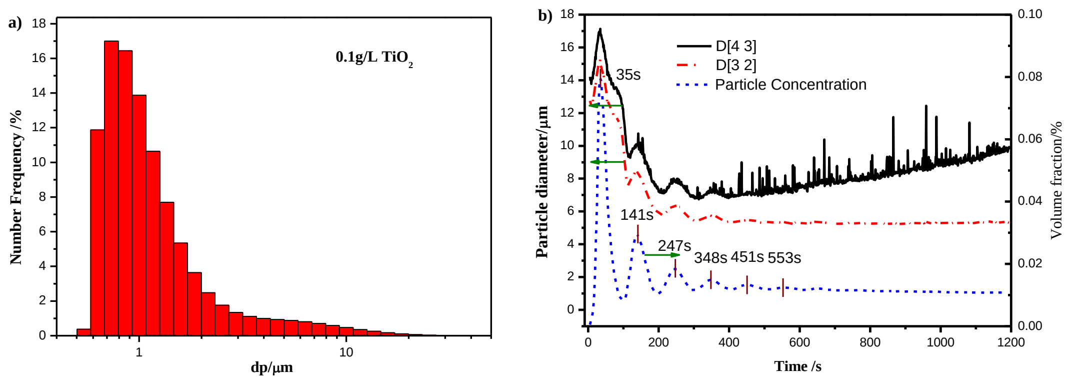

Fig 2 a) Particles size distribution of the P25-TiO_2 powder dispersed in water, b) Variation of various mean particle sizes and particle volume fraction with time.[47]

3. Numerical simulation of the nanoparticle-laden flow

3.1 Physical model for the tubular reactor

As has been mentioned above, the particle volume fraction has been measured by LD method, but only volume fraction cannot help us to know the mechanism of the particle transport phenomenon in such a circulating flow system. To explain the transport phenomenon of the particles in laminar circular flow, especially the details of the movement and variation of the particles with different size during the transport process, a simulation based on the Euler-Lagrange model was conducted. The geometry model for the simulation is showed in **Fig. 3a,** which is established according to the experimental set-up, but the particle size analyze and pump are neglected for the sake of simplicity. Here the main tube has a diameter of 30 mm with length of

0.5 m, and the connecting pipe has a diameter of 10 mm with length of 1.7m, which is the same with experimental set-up. The mesh used in this simulation is showed in **Fig 3b**, which is obtained from unstructured triangular grid. For the boundary layer, two layers of quadrilateral grids are adopted near the boundary. The mesh dependency analysis based on particle volume fraction was then conducted and the results are showed in **Fig.3d**. It turned out that the mesh with a grid number of 6212 is accurate enough for this simulation and also time-efficient.

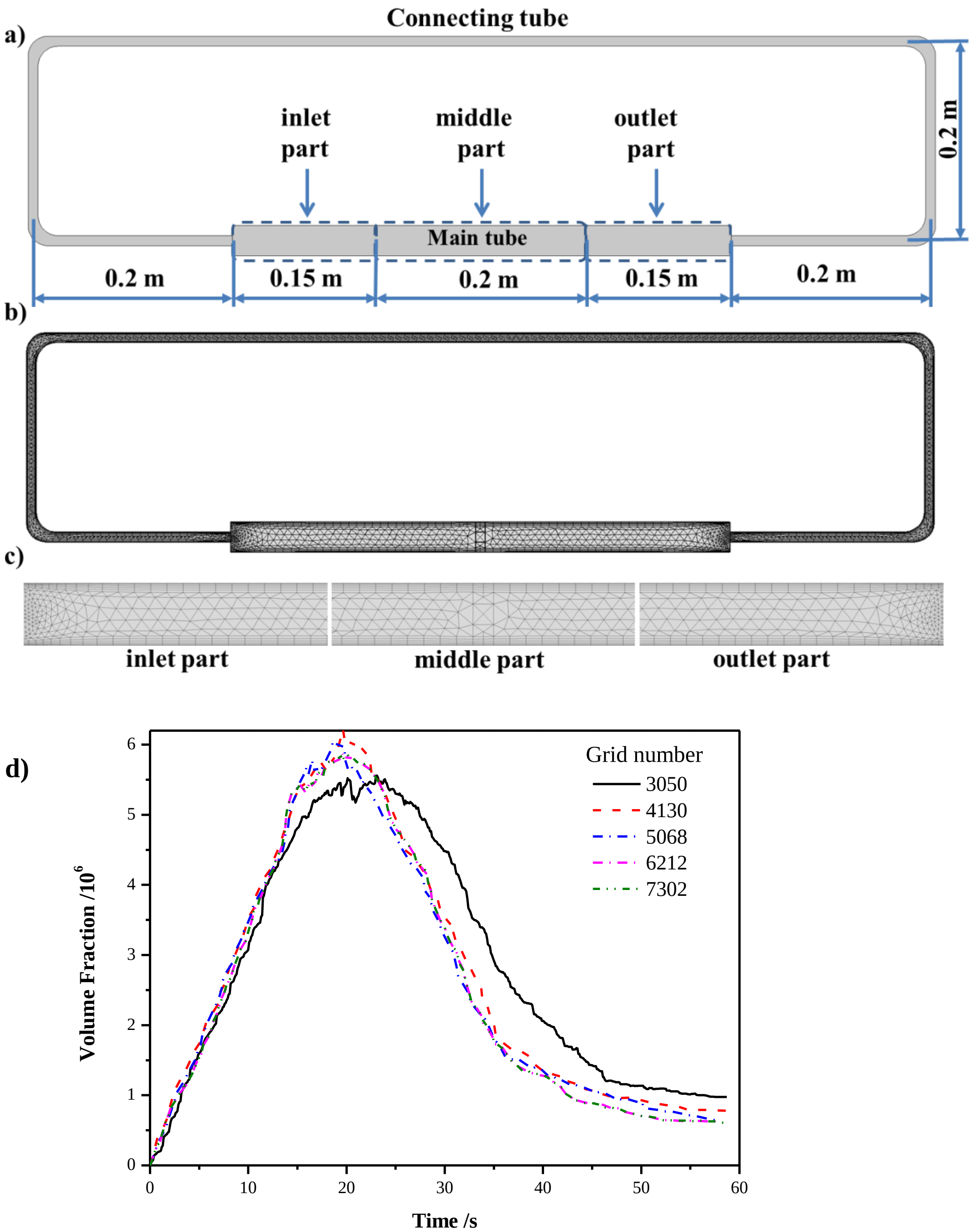

Fig.3 a) The Geometry model, **b)** computing mesh of the simulation, **c)** Local enlarged figure of the mesh, **d)** mesh dependency analysis based on particle volume fraction

On the other hand, as the particles movement will be described under the Lagrange viewpoint, the particles need to be traced one by one. However, it will be an extremely large amount of particles in the tube in practice, for example, the total volume of the channel is about 0.423 L, supposing the particles size is 3 μm and volume fraction is 0.01%, the amount of the particles will be 2.994×109, which is a too huge to cost an impossible computational resource. To solve this problem, only 10,000 particles are taken into account in the simulation, and these particles can present the migration principle of the particles with different size. For the convenience of analyzing, we also divided the main tube into three sections, i.e. inlet, middle and outlet sections, respectively. Furthermore, the properties of particles and the base fluid have significant influence on the interactions between particles and liquid and/or between particles and particles. The properties of particles mainly include density, shape, size, specific surface area and surface charge et al. The density of the P25 TiO_2 particles was defined as 4000 kg/m^3 according to Ref.[48], and the size of particle was defined as the particle size distribution as Fig. 2a shows which was obtained from the experimental data. The shape of the particles also has a significant impact on the drag force between liquid and solid phase, whereas the shape is often defined as spherical in numerical study to simply the computational model [54]. To solve this problem, some drag correlations have been developed to modify the influence of particle shape on drag force between particles and fluid [55,56]. In this study, as the particle was set as a common photocatalyst P25 TiO_2, and the SEM of this kind of particles shows that the morphology generally exhibits spherical [57], the particles in this study are all considered as spherical particles. And it needs to be further pointed out that if the current computational model is needed to simulate the other non-spherical particles, one merely need to add some corresponding drag correlations mentioned above. On the other hand, particle aggregation is a common phenomenon in suspension especially for tiny particles such as nanoparticles, and there are many influence factors of the aggregation phenomenon, such as the temperature of suspension, the pH of the suspension, ions in the base solution, particle size, shape, method of preparation and solid concentration [1,58]. Since the particle aggregation phenomenon has noticeable impact on many applications, there have been many theoretical [59-61] and experimental [62-64] studies focus on the problem. In this study, aggregation was also taken into account by introducing a real particle size distribution (PSD) which had been obtained from experimental data [47]. In other words, the particles aggregation was assumed to be equilibrium state and the particles in this study are aggregated secondary particles, thus the aggregation effect is taken into consideration in reality. Table 1 lists the parameters of particles and base liquid used in the computational model of this study.

Table 1 Some parameters of particles and base liquid used in the computational model

Parameters	Description
Particles	P25 TiO_2
Base fluid	Deionized water
Density of particles	4000 kg/m^3
Particle size	Using the PSD shown in **Fig. 2a**
Particle quantity in the model	10000
Density of the base fluid	1000 kg/m^3
Viscosity of the base fluid	1 $mPa \cdot s$

3.2 Mathematical model

Considering that the particles concentration is very low in our study, to simplify the mathematic model, we assume that the particles hardly influence the fluid field. Therefore, the simulation can be done in two steps. Firstly, a single phase flow in the geometry was solved and then the trajectory of particles was computed. In particular, in our case it is worth noting that the flow region is a closed circular channel, which only has wall boundary but not has inlet or outlet boundary. To solve this problem, the whole circular channel will be divided into two parts, the main tube and the connecting tube. The flow direction of the circular is set to be anticlockwise, so the right head of the connecting tube is set as the inlet boundary of the connecting tube which is also set as the outlet boundary of the main flow tube and the left end of the connecting tube is set as the outlet boundary which is also set as the inlet boundary of the main flow tube. The circular flowrate is set as 15 L/h which is the same as the experimental condition.

As has been noted, in our study the trajectory of particles will be computed by solving ordinary differential equations using Newton's law of motion. In this method, the particles are treated as point masses. The specification of particle diameter is mostly used for size-dependent forces, such as the drag and Brownian motion forces. As the particles concentration is very low in the liquid phase, it can be supposed that the liquid phase affects the motion of the particles but not vice-versa and one particle will not have obvious interactions with other particles. Thus, the particle tracing equation according to Newton's second law can be expressed as **Eq. (3)**:

$$\frac{d}{dt}\left(m_p \mathrm{v}\right) = \mathrm{F_D} + \mathrm{F}_g + \mathrm{F_B} \tag{3}$$

Where the m_p is the mass of the particle, the v is the velocity vector of particle; $\mathbf{F_D}$, $\mathbf{F_g}$ and $\mathbf{F_B}$ are three kinds of forces that can affect particles motion, and their calculation methods will be introduced in detail. $\mathbf{F_D}$ is the drag force of the fluid which is defined as:

$$\mathrm{F}_D = \left(\frac{1}{\tau_p}\right) m_p(\mathrm{u} - \mathrm{v}) \tag{4}$$

where the τ_p is the particle velocity response time, **u** is the velocity of the fluid, **v** is the velocity of the particle. There are a large number of expressions for the particle response time. It depends on the drag law, and selecting the appropriate drag law needs a consideration of the relative Reynolds number $\mathrm{Re_r}$ of particles in the flow, which is given by:

$$\mathrm{Re}_r = \frac{\rho \left\|\mathrm{u} - \mathrm{v}\right\| d_p}{\mu} \tag{5}$$

where the ρ and μ are the density and viscosity of the fluid, respectively, and d_p is the diameter of the particles. With the dimensionless number $\mathrm{Re_r}$, τ_p can be given by:

$$\tau_p = \frac{4\rho_p d_p^2}{3\mu C_D \mathrm{Re}_r} \tag{6}$$

where the C_D is the drag coefficient. Here, the parameter d_p is given by the particles size distribution shown in **Fig. 2a**. According to this particles size distribution, the range of the $\mathrm{Re_r}$ can be evaluated. As the drag force drives the particles to follow the fluids movement, the term $\left\|\mathrm{u} - \mathrm{v}\right\|$ that describe the difference between particle velocity and fluid velocity will be closed to 0 during the transport process, therefore the minimum value of the $\mathrm{Re_r}$ will be very clear to zero. On the other hand, if both the term $\left\|\mathrm{u} - \mathrm{v}\right\|$ and d_p reach the maximum value, the maximum of $\mathrm{Re_r}$ can be obtained. In this simulation, the maximum value of the $\left\|\mathrm{u} - \mathrm{v}\right\|$ most possibly happens at the initial state which the particles are static. And the maximum velocity of the fluid in the main tube can be calculated according to the velocity distribution of the laminar flow, and the value is 0.0118 m/s, so the maximum value of $\left\|\mathrm{u} - \mathrm{v}\right\|$ will be 0.0118 m/s. For the maximum particle size is 36.87 μm, the maximum value of the $\mathrm{Re_r}$ can be evaluated according to the Eq. 3, is

0.4203, that is, the range of the Re_r is 0-0.4203. According to the previous researches, the most common used drag law is the Stokes drag law, but it only can be used in the case that the Re_r <<1. Thus, another famous drag law called Oseen correction is used [65], which the drag coefficient is given by:

$$C_D = \frac{24}{Re_r}\left(1 + \frac{3}{16} Re_r\right) \tag{7}$$

$\mathbf{F_g}$ is the gravity force which is given by:

$$F_g = m_p \mathbf{g} \frac{(\rho_p - \rho)}{\rho_p} \tag{8}$$

$\mathbf{F_B}$ is the Brownian Force which can describe the Brownian motion of the particles. Actually, the Brownian motion of the particles leads to spreading of particles from regions of high particle concentration to low concentration. The expression of the Brownian Force is:

$$F_B = \zeta \sqrt{\frac{6\pi k_B \mu T d_p}{\Delta t}} \tag{9}$$

where the Δt is the time step taken by the solver, T is the absolute fluid temperature , k_B is the Boltzmann constant and the value is 1.3806×10^{-23} J/K, and ζ is a normally distributed random number with a mean of zero and unit standard deviation which is created for each particle, at each time step.

3.3 Model validation

To validate the model, the result of the variation of the particle volume with time by this simulation is compared with the experimental result, which is showed in **Fig 4**. As has been mentioned above, the particle volume fraction in the simulation is much smaller than the experimental condition for the huge computational source consumption, the particle volume fraction in **Fig 4** is normalized by dividing the mean particle volume fraction in the quasi-steady state. Also, for it has some simplified assumptions in the physical model, so the times of the two results are not exactly equivalent, therefore a normalized time is used by dividing the period of the oscillation curve, T. From the **Fig 4**, one can find that the tendencies of two curves are very similar in the first 3 periods, but it can be also seen that the continuity of the simulation curve is poor compared with the experimental results, this may due to the particle amount is much smaller than the experimental condition. However, in this study, we only want to reveal the particle movement mechanism and how this movement results in an oscillation of particle volume fraction and mean particle size. From this viewpoint, the result of this simulation result also exhibit a very obvious oscillation tendency, so it can help us to understand the mechanism.

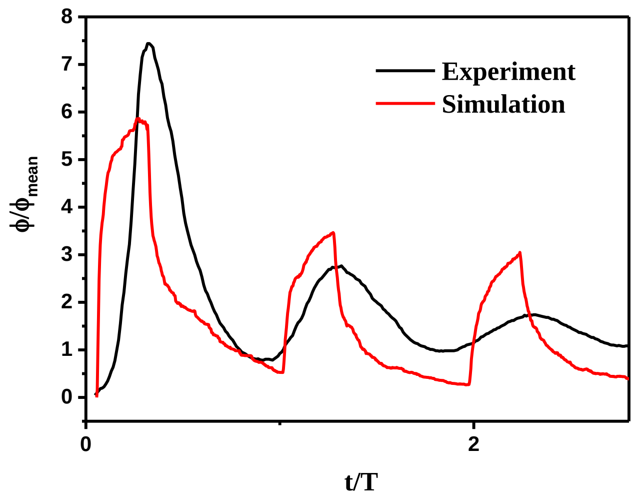

Fig. 4. Vatiation of particle volume fraction with time in experiment and simulation

4. Results and discussion

4.1 The flow field of the particle-laden flow in the circulating flow system

As the particles moving in the fluids are significantly affected by the drag force of fluid, the flow field of the flow is believed to be extremely important for the latter analysis of particles movement. The velocity distribution obtained by the simulation is showed in **Fig. 5**, which is a typical laminar tube flow. **Fig. 5b** shows the velocity distribution in the inlet part, and it can be seen that the fluid flow from the thinner connecting tube into the thicker main tube. As the fluid velocity is larger in the thinner connecting tube, there is a high velocity region in the front-end of the inlet part, and there also appears inverse flow with two symmetrical vortexes in the top and the bottom of this region. Then the fluid flow in the main tube gradually passes into the fully developed flow. **Fig. 5c** shows the velocity distribution in the middle part, which shows the character of fully developed flow. And the velocity distribution exhibits a parabolic distribution, which is a typical laminar tube flow. This kind of flow has a character that the velocity in the center of tube reaches the maximum value, while the velocity near the wall is low and the velocity at wall is zero. That is to say, the velocity distribution shows an obvious difference in radial direction. And **Fig. 5d** shows the velocity distribution in the outlet part, and it can be seen that the velocity distribution in the front of this part is very similar to the middle part. However, it appears a high velocity region in the last end of this part, for the fluid flow from the thicker main tube to the thinner connecting tube.

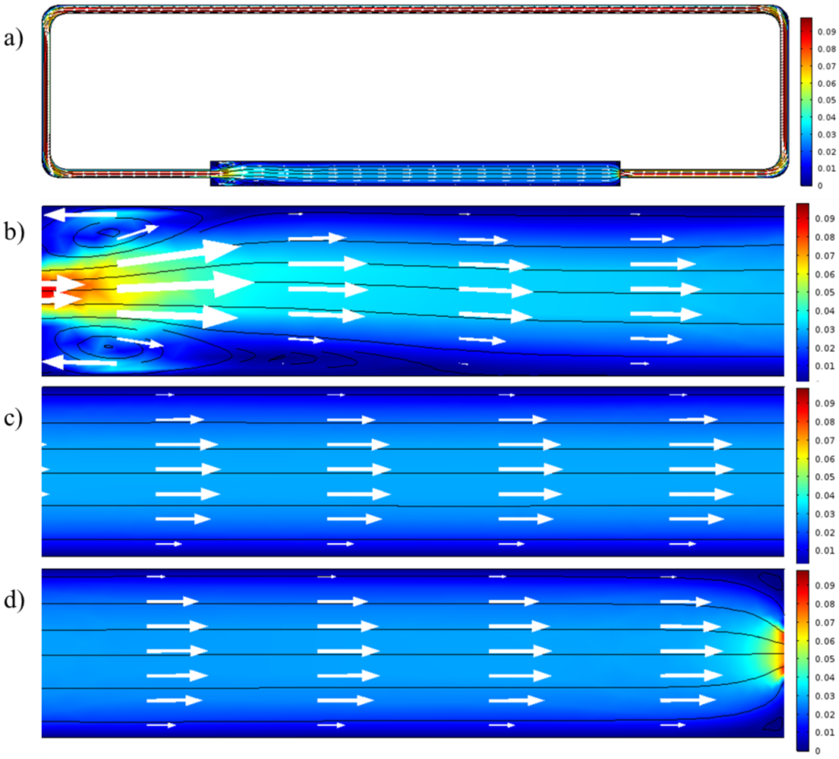

Fig.5 Contour of the velocity magnitude of the circular flow with streamlines **a)**the whole channel, **b)** the inlet part c)the middle part **d)**the outlet part, of the main tube

4.2 Particle volume fraction

Fig. 6 shows the variation of the average particle concentration with time during the transport process in three parts of the tube. As has been mentioned in section 3.3, the simulation result is very similar to the experimental results. The most obvious difference between the two results is that the curve of the experiment reaches a constant value in the end, whereas the curve of the simulation just holds a value in a small range. This deviation may be due to that too fewer particles are taken into account in the simulation and the disturbance from pump or other equipment used in experiment has also not been taken into account. However, as the tendency obtained from the simulation is similar to the experiment results, it is therefore reasonable to use the results of simulation to find the mechanism of the observed experimental phenomenon. From Fig 6, it can be found that the highest peak appears at the first peak of the oscillation curve in all the three part of main tube, while the height of the three peaks are different and the peak in the inlet part is the highest. It can also been seen that the peaks of the oscillation curves in different parts also don't coincide in time. These phenomena may mean that the oscillation of particle volume fraction is caused by the particle movement in the circulating flow. And to verify this assumption, we will discuss the particle distribution and trajectory in the next part.

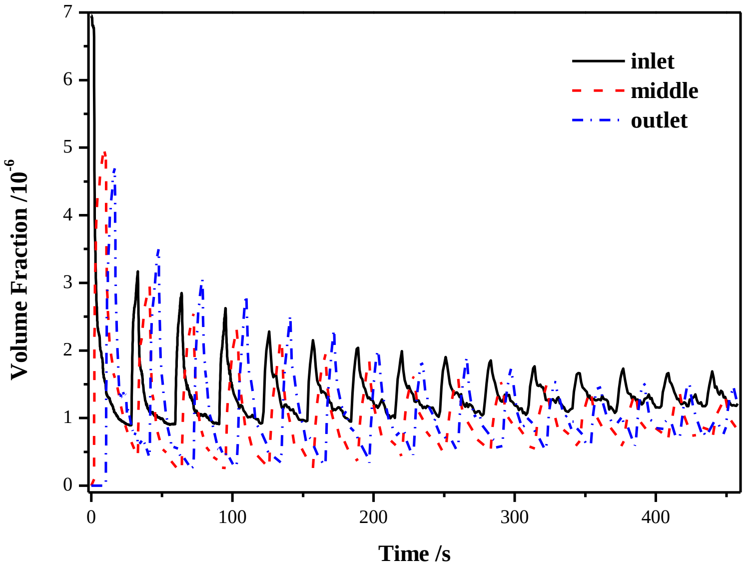

Fig. 6 Variation of volume fraction of particles with time derived from the simulation

4.3 The particle trajectory

Firstly, the trajectories of particles in the times which correspond to the position of the peaks of the particle volume fraction curve are showed in **Fig 7**. It can be found that the particles distribution exhibits a parabolic like state in the initial time which is very similar to the velocity distribution shown in the **Fig 5**. And it can be easily found from **Fig 7a-f** that the particles in these peak times tend to arrange in a parabolic curve. Combined with the velocity distribution mentioned above, it can be inferred that this phenomenon is caused by the parabolic distribution of radial velocity, that is, the particles near the center will have higher velocity, while the particles near the wall will move slowly. Thus, the particles with higher velocity will pass through the whole circulating system much faster than other particles, and when they reach the counting region, there will be a relative higher particle volume fraction. This process is believed to be a good explanation for the oscillation phenomenon. Furthermore, it can be found that the parabolic shape of particles gets narrower gradually until it almost turns into a line at the quasi-steady state, and this is due to the distance between the particles with different velocity will be longer as time goes on. The narrower parabolic particles arrangement means fewer particles, which can explain the lower and lower peaks high in the oscillation curve. Also, it can be found that the position of the overall parabolic shape in the tube becomes lower and lower during the transport process, which may due to the gravity force of the particles. After several circles, particles moving in the main tube will gather in the positions that a little lower than the axis of the main tube.

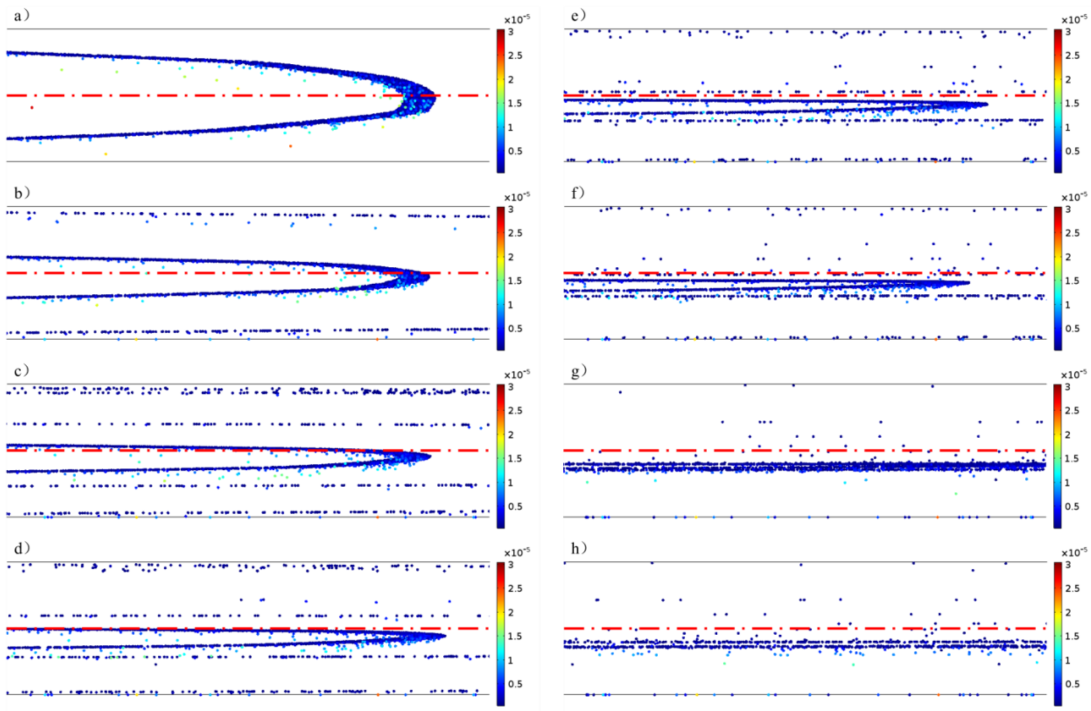

Fig. 7 schematic of the particles position in the peak times and the quasi-steady state **a)** t=14.6s **b)** t=45.6s **c)** t=76.7 s **d)** t=108 s **e)** t=139 s **f)** t=170 s **g)** t= 360 s **h)** t=400 s

Fig 8 shows the trajectory and evolution process of a single particle counted from the simulation result. For there are so many particles in the tube, we just choose four particles which we think are very representative, and the particles size are 0.496 μm, 1.117 μm, 10.842 μm and 15.043 μm，respectively. We compute the locations of particles in the main tube at any time. As the particles moves in the circulating system, we also distinguished the different number of cycles of the particle trajectory. The particle with size of 0.496 μm is selected to represent the little particle and it can be found that its trajectory in the middle part is almost a straight line. At the same time, we also found that in the first 10 cycles, the particle trajectory showed a gradual downward trend, but after the 10_{th} cycle, the particle trajectory remained almost unchanged. In addition, we also selected the particles with a diameter of 1.117 μm and this part of particles is treated as median-sized particles. From the **Fig 8 b)**, we can see that the trajectory of this kind of particles is very similar to that of 0.496 μm particle, which looks straight in the middle part, and will basically stabilize in one trajectory after the 10_{th} cycle. Furthermore, we can conclude that the motion character of the last mentioned two kinds of particles is that they follow the fluid and keep moving on a straight line in the main tube, that is to say, the settling velocity generated by gravity is very small. After the discussion of small particles, it is necessary to discuss the large particle. Therefore, particle with size of 10.842 μm is also selected. It can be found that this kind of particle is seriously affected by gravity, or the trajectory of this particle in the middle part of the main tube is in the downward inclination. And with the increase of the number of cycles, its trajectory in the main tube shows a very obvious downward trend even after 10_{th} cycles. Finally, we chose the particle size of 15.043 μm, because this particle is the largest particle which is still in motion at 400 s in this simulation and can represent the coarse particle. It can be seen that the effect of gravity on the particle is more obvious, and the downward inclination of its trajectory in the main tube is more obvious. But for this particle, we can only take 10 cycles, because the settlement occurred before the 16_{th} cycle, which shows that such particles in the pipeline cannot maintain a continuous circulating movement, and eventually will settle down.

4.4 Particle size distribution

The particle size distribution in the different parts of the main tube counted from the simulation results is showed in **Fig. 9**. Both of the number and volume particle size distributions are taken into account, also the three parts of the tube are computed respectively. For the convenience of description, according to the results in the section 4.3, we can call particles of 1-10 μm as small particles, and particles of more than 10 μm as large particles. It can be found that the volume particle size distribution is a unimodal distribution at the first peak. As the time goes on, the particle size distribution curve gradually becomes an obvious bimodal distribution. If one look at the position and corresponding size of the two peaks separately, one can see that the peak of large particles moves to the left with time, and the height of it increases obviously with time. This trend also proves that the particles with a diameter more than 15 μm are greatly affected by gravity and easy to settle down, which results in some loss of the particles. Therefore, the particles with a diameter slightly smaller than 15 μm occupy a higher volume fraction in the large particles, and it form the peak of large particles in the particle size distribution curve. In addition, it can be seen that the position of the peak of small particles gradually move to left with time. This phenomenon shows that the small particles almost have no loss in the transport process; as a result, volume frequency of this part of particles has obvious advantages especially when the large particles lost.

And it can be also seen that the particles size distribution based on number seems not have much change on the different times of the peaks as the experiment shows, associated with **Fig 7**, we further confirm that the group of particles which have the higher velocity will repeat to appear on the region for counting, so the number particles size distribution is almost no change.

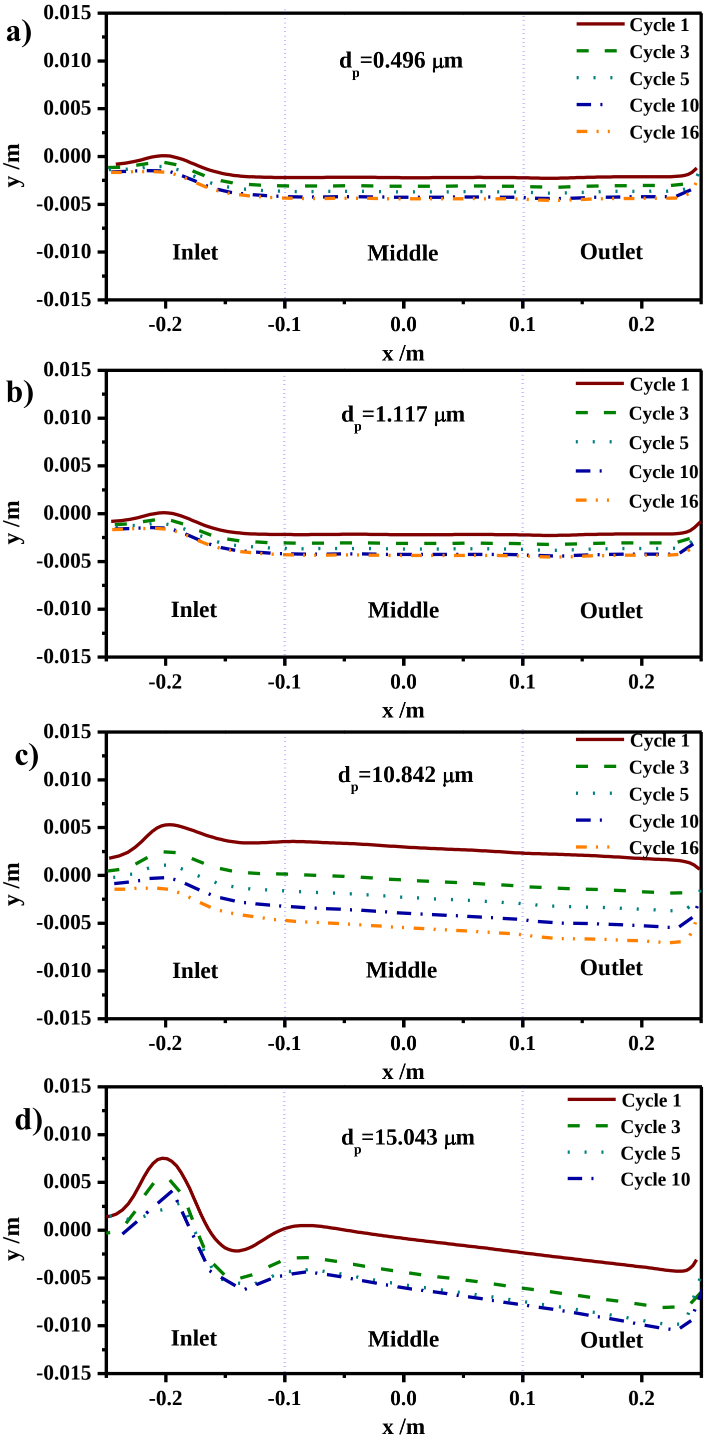

Fig 8 particles motion trace in the main tube **a)** d_p=0.496 μm, **b)** d_p =1.117μm **c)** d_p =10.842μm, **d)** d_p =15.043μm

From the prospective of photocatalytic reaction, amount of the particles especially the smaller particles are more benefit to the reaction efficiency. The result derived from the simulation inspires that in the circulating system, effects of gravity is only remarkable for the large particles which the size are more than 10 μm, and a very low circulating flowrate such as 15 L/h is enough to make sure the small particles keep suspending. And for the amount of the small particles are quite larger than that of large particles, adopting a lower flowrate in the photocatalytic application is reasonable and also energy efficient.

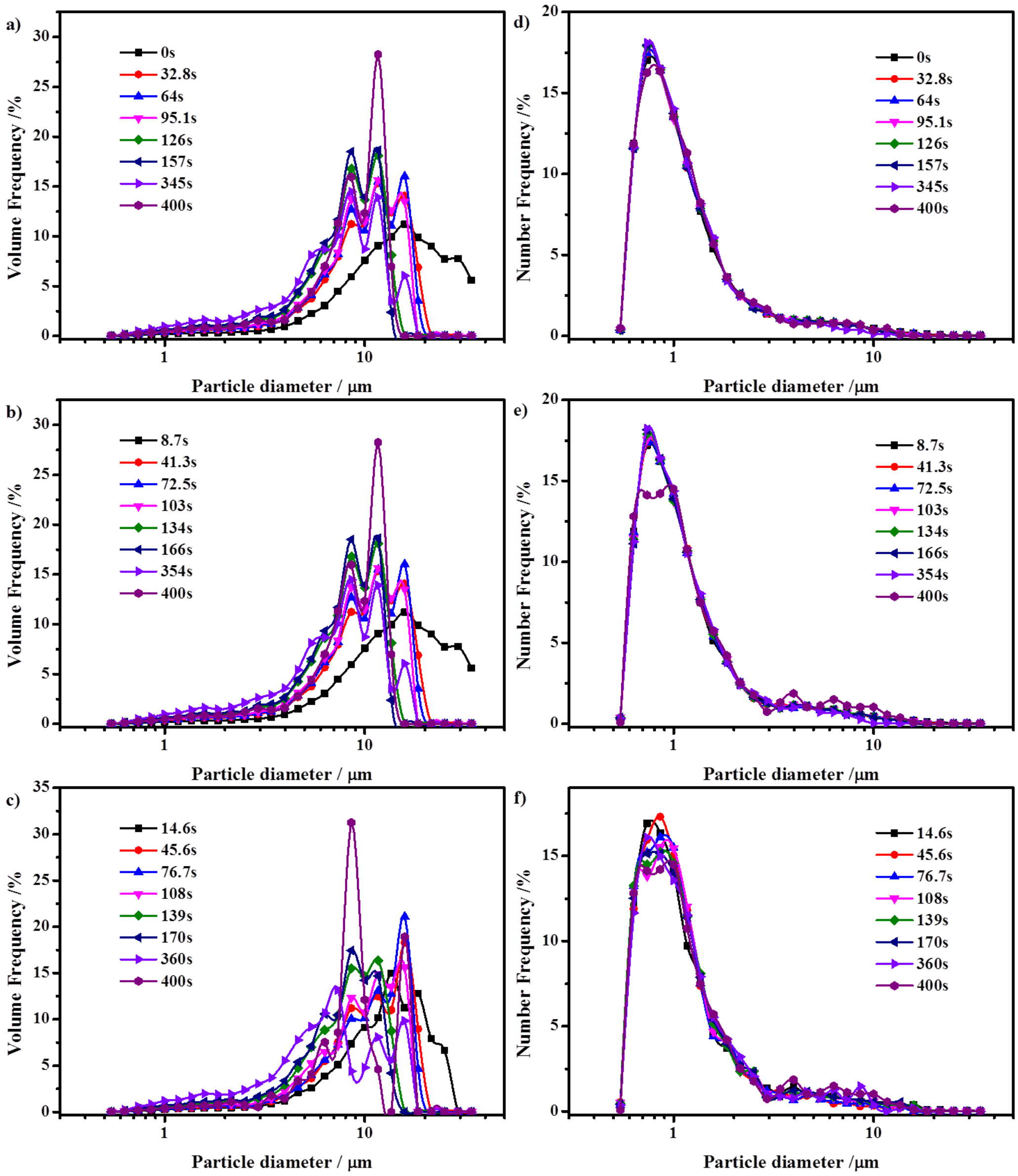

Fig.9 Particles size distribution based on volume obtained from **a)** inlet part, **b)** middle part, **c)** outlet part, and Particles size distribution based on number obtained from **d)** inlet part, **e)** middle part, **f)** outlet part

5 Conclusions

The suspension of micro- or nanoscale particles in liquid is used widely and the circulating flow is also regularly chosen as the flow form in the application of this kind of two-phase fluid. In this study, a DEM method is used in a simulation of the circulating laminar flow system to explain the transport phenomenon of particles. It can be found the particle concentration and size distribution varies with time and appears periodical oscillation, which is related to the non-uniform velocity distribution of particles in the radial direction of tube. In this process, the particle size distribution changes from unimodal distribution to bimodal distribution, for the particles with a size less than 10 μm almost have no loss in the transport process. Furthermore, particles tend to gather in the middle region of the tube after several cycles, which is also the region with the higher velocity in the shear flow. Also, with the effects of gravity force, the integral particles group tends to distribute in the region a little lower than the center.

As a case study, this study mainly focus on the particle transport phenomenon in photocatalytic reactor, so the kind of particles and base liquid, operating mode, initial condition and other parameters were specified to photocatalytic reactor. However, this simulation can also be extended to other applications, such as heat transfer enhancement by nanofluid, general solid-liquid reaction et al. And it can be implemented by simply replacing some parameters or introducing some correlations in the existing model, which is believed to be useful for understanding the particle transport phenomenon in different applications.

Acknowledgements

The authors gratefully acknowledge the financial support of the National Natural Science Foundation of China (No. 51776165, 51888103) and the financial support from Royal Society-Newton Advanced Fellowship grant (NAF\R1\191163).

References:

[1] Jing DW, Song DX. Optical properties of nanofluids considering particle size distribution: Experimental and theoretical investigations. RENEW SUST ENERG REV. 2017; 78:452-65.

[2] Kudo A, Miseki Y. Heterogeneous photocatalyst materials for water splitting. CHEM SOC REV. 2009; 38:253-78.

[3] Jing DW, Guo LJ, Zhao L, Zhang XM, Liu H, Li MT, et al. Efficient solar hydrogen production by photocatalytic water splitting: From fundamental study to pilot demonstration. INT J HYDROGEN

ENERG. 2010; 35:7087-97.

[4] Vajjha RS, Das DK. A review and analysis on influence of temperature and concentration of nanofluids on thermophysical properties, heat transfer and pumping power. INT J HEAT MASS TRAN. 2012; 55:4063-78.

[5] Fajrina N, Tahir M. A critical review in strategies to improve photocatalytic water splitting towards hydrogen production. INT J HYDROGEN ENERG. 2019; 44:540-77.

[6] Kim SJ, Bang IC, Buongiorno J, Hu LW. Effects of nanoparticle deposition on surface wettability influencing boiling heat transfer in nanofluids. APPL PHYS LETT. 2006; 89:153107.

[7] KUDO A. Development of photocatalyst materials for water splitting. INT J HYDROGEN ENERG. 2006; 31:197-202.

[8] Luo B, Song R, Jing D. ZnCr LDH nanosheets modified graphitic carbon nitride for enhanced photocatalytic hydrogen production. INT J HYDROGEN ENERG. 2017; 42:23427-36.

[9] Pulido Melián E, González Díaz O, Ortega Méndez A, López CR, Nereida Suárez M, Doña Rodríguez JM, et al. Efficient and affordable hydrogen production by water photo-splitting using TiO2-based photocatalysts. INT J HYDROGEN ENERG. 2013; 38:2144-55.

[10] Ma Z, Cui Z, Lv Y, Sa R, Wu K, Li Q. Three-in-One: Opened Charge-transfer channel, positively shifted oxidation potential, and enhanced visible light response of g-C3N4 photocatalyst through K and S Co-doping. INT J HYDROGEN ENERG. 2020; 45:4534-44.

[11] Fang W, Shangguan W. A review on bismuth-based composite oxides for photocatalytic hydrogen generation. INT J HYDROGEN ENERG. 2019; 44:895-912.

[12] Li X, Yu J, Low J, Fang Y, Xiao J, Chen X. Engineering heterogeneous semiconductors for solar water splitting. J MATER CHEM A. 2015; 3:2485-534.

[13] Ren YX, Zhao L, Jing DW, Guo LJ. Investigation and modeling of CPC based tubular photocatalytic reactor for scaled-up hydrogen production. INT J HYDROGEN ENERG. 2016; 41:16019-31.

[14] Cao F, Liu H, Wei Q, Zhao L, Guo L. Experimental study of direct solar photocatalytic water splitting for hydrogen production under natural circulation conditions. INT J HYDROGEN ENERG. 2018; 43:13727-37.

[15] Yang Y, Wei Q, Hou J, Liu H, Zhao L. Solar concentrator with uniform irradiance for particulate photocatalytic hydrogen production system. INT J HYDROGEN ENERG. 2016; 41:16040-7.

[16] Wei Q, Yang Y, Liu H, Hou J, Liu M, Cao F, et al. Experimental study on direct solar photocatalytic water splitting for hydrogen production using surface uniform concentrators. INT J HYDROGEN ENERG. 2018; 43:13745-53.

[17] Li L, Chen R, Liao Q, Zhu X, Wang G, Wang D. High surface area optofluidic microreactor for redox mediated photocatalytic water splitting. INT J HYDROGEN ENERG. 2014; 39:19270-6.

[18] Yan H, Yang J, Ma G, Wu G, Zong X, Lei Z, et al. Visible-light-driven hydrogen production with extremely high quantum efficiency on Pt‑PdS/CdS photocatalyst. J CATAL. 2009; 266:165-8.

[19] Liu M, Wang L, Max Lu G, Yao X, Guo L. Twins in Cd1−xZnxS solid solution: Highly efficient photocatalyst for hydrogen generation from water. ENERG ENVIRON SCI. 2011; 4:1372.

[20] Dong Q, Fang Y, Shao Y, Mulligan P, Qiu J, Cao L, et al. Metal-free efficient photocatalyst for stable visible water splitting via a two-electron pathway. . SCIENCE. 2015; 347:967-70.

[21] Wang Q, Hisatomi T, Jia Q, Tokudome H, Zhong M, Wang C, et al. Scalable water splitting on particulate photocatalyst sheets with a solar-to-hydrogen energy conversion efficiency exceeding 1%. NAT MATER. 2016; 15:611-5.

[22] Barresi A, Baldi G. Solid dispersion in an agitated vessel effect of particle shape and density. CHEM ENG SCI. 1987; 12:2969-72.

[23] Huang JK, Lu YJ, Wang H. A new quantitative measurement method for mixing and segregation of binary-mixture fluidized bed by capacitance probe. CHEM ENG J. 2017; 326:99-108.

[24] Wang K, Liu G, Liu ZG, Wu J, Yi LT, Zhang JL, et al. Acoustic sensor approaches for sand detection in sand–water two-phase flows. POWDER TECHNOL. 2017; 320:739-47.

[25] Felder S, Chanson H. Phase-detection probe measurements in high-velocity free-surface flows including a discussion of key sampling parameters. EXP THERM FLUID SCI. 2015; 61:66-78.

[26] Nocentini M, Pinelli D, Magelli F. Dispersion coefficient and settling velocity of the solids in agitated slurry reactors stirred with multiple rushton turbines. CHEM ENG SCI. 2002; 57:1877-84.

[27] Roshani GH, Nazemi E, Feghhi SAH, Setayeshi S. Flow regime identification and void fraction prediction in two-phase flows based on gamma ray attenuation. MEASUREMENT. 2015; 62:25-32.

[28] Xu YQ, Xu CB, Guan ZC, Liu YW, Tian Y, Sheng YN, et al. Numerical simulation method of ultrasonic wave propagation in gas-liquid two-phase flow of deepwater riser. MECH SYST SIGNAL PR. 2019; 118:78-92.

[29] Liu L, Fang ZY, Wu YP, Lai XP, Wang P, Song K. Experimental investigation of solid-liquid two-phase flow in cemented rock-tailings backfill using Electrical Resistance Tomography. CONSTR BUILD MATER. 2018; 175:267-76.

[30] Black DL, McQuay MQ, Bonin MP. Laser-based techniques for particle-size measurement: A review of sizing methods and their industrial applications. PROG ENERG COMBUST. 1996; 22:267-306.

[31] Levoguer C. Using laser diffraction to measure particle size and distribution. MET POWDER REP. 2013; 68:15-8.

[32] Ma ZH, Merkus HG, de Smet J, Heffels C, Scarlett B. New developments in particle characterization by laser diffraction: size and shape. POWDER TECHNOL. 2000; 111:66-78.

[33] Hu XW, Guo LJ. Numerical investigations of catalyst–liquid slurry flow in the photocatalytic reactor for hydrogen production based on algebraic slip model. INT J HYDROGEN ENERG. 2010; 35:7065-72.

[34] Hatami M, Hosseinzadeh K, Domairry G, Behnamfar MT. Numerical study of MHD two-phase Couette flow analysis for fluid-particle suspension between moving parallel plates. J TAIWAN INST CHEM E. 2014; 45:2238-45.

[35] Hedayati F, Domairry G. Nanoparticle migration effects on fully developed forced convection of TiO2–water nanofluid in a parallel plate microchannel. PARTICUOLOGY. 2016; 24:96-107.

[36] Feng YQ, Yu AB. Assessment of Model Formulations in the Discrete Particle Simulation of Gas−Solid Flow. IND ENG CHEM RES. 2004; 43:8378-90.

[37] Morris JF, Brady JF. Pressure-driven flow of a suspension: Buoyancy effects. INT J MULTIPHAS FLOW. 1998; 24:105-30.

[38] Peng ZB, Doroodchi E, Evans G. DEM simulation of aggregation of suspended nanoparticles. POWDER TECHNOL. 2010; 204:91-102.

[39] Chaumeil F, Crapper M. Using the DEM-CFD method to predict Brownian particle deposition in a constricted tube. PARTICUOLOGY. 2014; 15:94-106.

[40] Jing DW, Liu H, Zhang XH, Zhao L, Guo LJ. Photocatalytic hydrogen production under direct solar light in a CPC based solar reactor: Reactor design and preliminary results. ENERG CONVERS MANAGE. 2009; 50:2919-26.

[41] Li D, Xiong K, Li W, Yang ZH, Liu C, Feng X, et al. Comparative Study in Liquid-Phase Heterogeneous Photocatalysis: Model for Photoreactor Scale-Up. IND ENG CHEM RES. 2010; 49:8397-405.
[42] Malato S, Blanco J, Vidal A, Richter C. Photocatalysis with solar energy at a pilot-plant scale: an overview. APPL CATAL B-ENVIRON. 2002; 37:1-15.
[43] Ochoa-Gutiérrez KS, Tabares-Aguilar E, Mueses MÁ, Machuca-Martínez F, Li Puma G. A Novel Prototype Offset Multi Tubular Photoreactor (OMTP) for solar photocatalytic degradation of water contaminants. CHEM ENG J. 2018; 341:628-38.
[44] Xing Z, Zong X, Pan J, Wang LZ. On the engineering part of solar hydrogen production from water splitting: Photoreactor design. CHEM ENG SCI. 2013; 104:125-46.
[45] Cao F, Liu H, Wei Q, Zhao L, Guo L. Experimental study of direct solar photocatalytic water splitting for hydrogen production under natural circulation conditions. INT J HYDROGEN ENERG. 2018; 43:13727-37.
[46] Segré G, Silberberg A. Behaviour of macroscopic rigid spheres in Poiseuille flow Part 2. Experimental results and interpretation. J FLUID MECH. 1962; 14:136.
[47] Geng J, Tang J, Wang Y, Huang Z, Jing D, Guo L. Attenuated Periodical Oscillation Characteristics in a Nanoscale Particle-Laden Laminar Flow. IND ENG CHEM RES. 2020; 59:8018-27.
[48] Kalantary RR, Shahamat YD, Farzadkia M, Esrafili A, Asgharnia H. Photocatalytic degradation and mineralization of diazinon in aqueous solution using nano-TiO2(Degussa, P25): kinetic and statistical analysis. DESALIN WATER TREAT. 2015; 55:555-63.
[49] Cao F, Wei QY, Liu H, Lu N, Zhao L, Guo LJ. Development of the direct solar photocatalytic water splitting system for hydrogen production in Northwest China: Design and evaluation of photoreactor. RENEW ENERG. 2018; 121:153-63.
[50] Wei QY, Yang Y, Hou JY, Liu H, Cao F, Zhao L. Direct solar photocatalytic hydrogen generation with CPC photoreactors: System development. SOL ENERGY. 2017; 153:215-23.
[51] Jing DW, Liu H, Zhang XH, Zhao L, Guo LJ. Photocatalytic hydrogen production under direct solar light in a CPC based solar reactor: Reactor design and preliminary results. ENERG CONVERS MANAGE. 2009; 50:2919-26.
[52] Kowalczuk PB, Drzymala J. Physical meaning of the Sauter mean diameter of spherical particulate matter. PARTICUL SCI TECHNOL. 2016; 34:645-7.
[53] Wang L, Fang NF, Yue ZJ, Shi ZH, Hua L. Raindrop Size and Flow Depth Control Sediment Sorting in Shallow Flows on Steep Slopes. WATER RESOUR RES. 2018; 54:9978-95.
[54] Song D, Yang Y, Jing D. Insight into the contribution of rotating Brownian motion of nonspherical particle to the thermal conductivity enhancement of nanofluid. INT J HEAT MASS TRAN. 2017; 112:61-71.
[55] Cao Z, Tafti DK, Shahnam M. Development of drag correlation for suspensions of ellipsoidal particles. POWDER TECHNOL. 2020; 369:298-310.
[56] Liu X, Gan J, Zhong W, Yu A. Particle shape effects on dynamic behaviors in a spouted bed: CFD-DEM study. POWDER TECHNOL. 2020; 361:349-62.
[57] Jin J, Li X, Geng J, Jing D. Insights into the complex interaction between hydrophilic nanoparticles and ionic surfactants at the liquid/air interface. PHYS CHEM CHEM PHYS. 2018; 20:15223-35.
[58] French RA, Jacobson AR, Kim B, Isley SL, Penn RL, Baveye PC. Influence of Ionic Strength, pH,

and Cation Valence on Aggregation Kinetics of Titanium Dioxide Nanoparticles. ENVIRON SCI TECHNOL. 2009; 43:1354-9.

[59] Song D, Hatami M, Wang Y, Jing D, Yang Y. Prediction of hydrodynamic and optical properties of TiO 2 /water suspension considering particle size distribution. INT J HEAT MASS TRAN. 2016; 92:864-76.

[60] Jing D, Hu S, Zhang Y, Luo J. A modified diffusion-limited cluster aggregation model for accurate prediction of the coagulation and fragmentation process in nanoparticle suspension. J PHYS D APPL PHYS. 2019; 52:455305.

[61] Kumar S, Ramkrishna D. On the solution of population balance equations by discretization—I. A fixed pivot technique. CHEM ENG SCI. 1996; 51:1311-32.

[62] Chowdhury I, Duch MC, Mansukhani ND, Hersam MC, Bouchard D. Colloidal Properties and Stability of Graphene Oxide Nanomaterials in the Aquatic Environment. ENVIRON SCI TECHNOL. 2013; 47:6288-96.

[63] Luo B, Song R, Jing D. Particle aggregation behavior during photocatalytic ethanol reforming reaction and its correlation with the activity of H2 production. COLLOID SURFACE A. 2017; 535:114-20.

[64] Ebini RH, Sorensen CM. Light scattering studies of the sol-to-gel transition in particulate systems. J COLLOID INTERF SCI. 2019; 556:577-83.

[65] Yang M, Li S, Marshall JS. Effects of long-range particle‑particle hydrodynamic interaction on the settling of aerosol particle clouds. J AEROSOL SCI. 2015; 90:154-60.